30

SATELLITE & MESOMETEOROLOGY
RESEARCH PROJECT

Department of the Geophysical Sciences
The University of Chicago

EVALUATION OF ERRORS IN THE GRAPHICAL RECTIFICATION OF SATELLITE PHOTOGRAPHS

by

Tetsuya Fujita

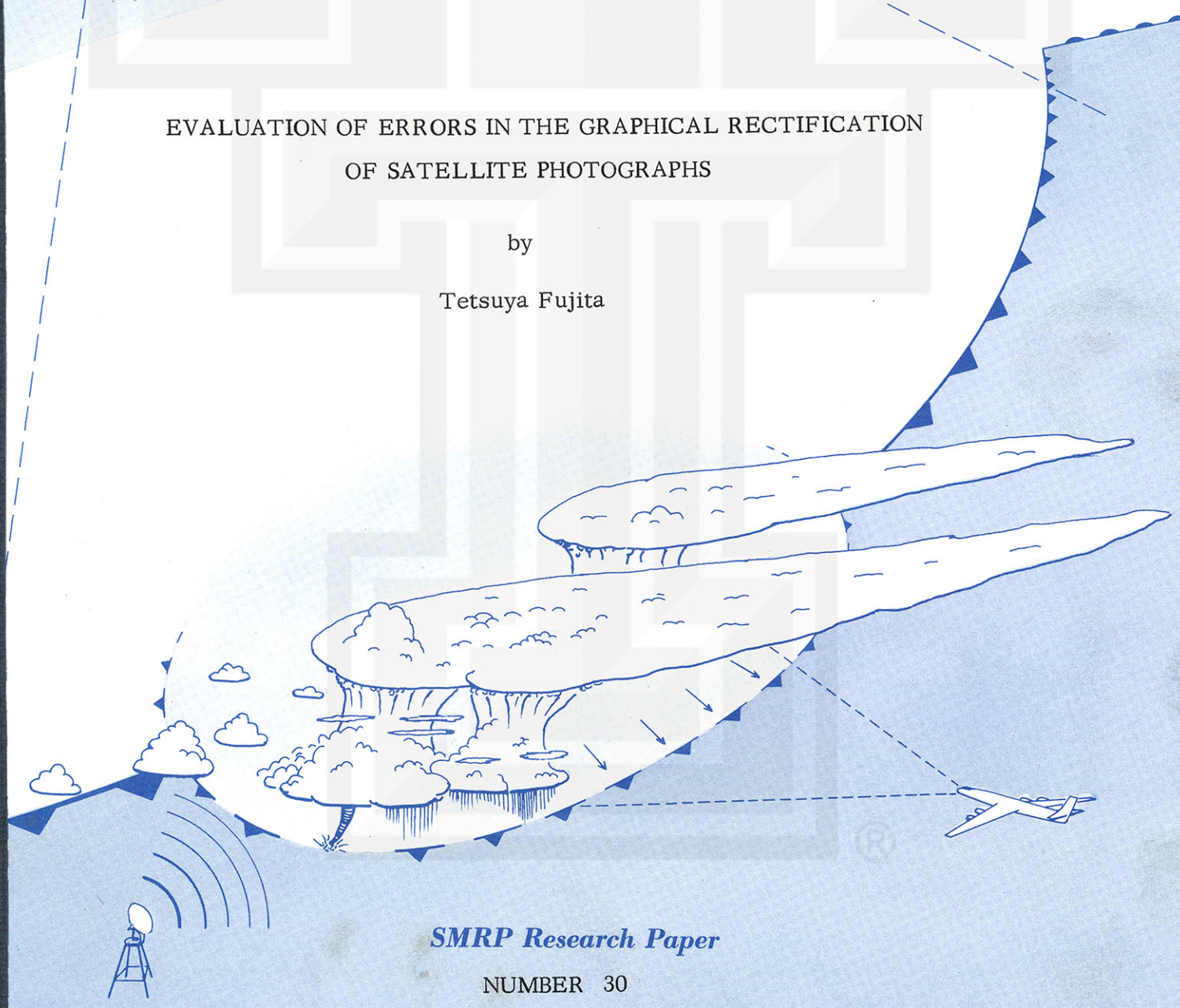

SMRP Research Paper

NUMBER 30

July 1964

1.* Report on the Chicago Tornado of March 4, 1961 - Rodger A. Brown and Tetsuya Fujita

2.* Index to the NSSP Surface Network - Tetsuya Fujita

3.* Outline of a Technique for Precise Rectification of Satellite Cloud Photographs - Tetsuya Fujita

4.* Horizontal Structure of Mountain Winds - Henry A. Brown

5.* An Investigation of Developmental Processes of the Wake Depression Through Excess Pressure Analysis of Nocturnal Showers - Joseph L. Goldman

6.* Precipitation in the 1960 Flagstaff Mesometeorological Network - Kenneth A. Styber

7.** On a Method of Single- and Dual-Image Photogrammetry of Panoramic Aerial Photographs - Tetsuya Fujita

8. A Review of Researches on Analytical Mesometeorology - Tetsuya Fujita

9. Meteorological Interpretations of Convective Nephsystems Appearing in TIROS Cloud Photographs - Tetsuya Fujita, Toshimitsu Ushijima, William A. Hass, and George T. Dellert, Jr.

10. Study of the Development of Prefrontal Squall-Systems Using NSSP Network Data - Joseph L. Goldman

11. Analysis of Selected Aircraft Data from NSSP Operation, 1962 - Tetsuya Fujita

12. Study of a Long Condensation Trail Photographed by TIROS I - Toshimitsu Ushijima

13. A Technique for Precise Analysis of Satellite Data; Volume I - Photogrammetry (Published as MSL Report No. 14) - Tetsuya Fujita

14. Investigation of a Summer Jet Stream Using TIROS and Aerological Data - Kozo Ninomiya

15. Outline of a Theory and Examples for Precise Analysis of Satellite Radiation Data - Tetsuya Fujita

* Out of print
** To be published

(Continued on back cover)

SATELLITE AND MESOMETEOROLOGY RESEARCH PROJECT

Department of the Geophysical Sciences

The University of Chicago

EVALUATION OF ERRORS IN THE GRAPHICAL RECTIFICATION OF SATELLITE PHOTOGRAPHS

by

Tetsuya Fujita

SMRP Research Paper # 30

The research reported in this paper has been supported by the National Weather Satellite Center, U.S. Weather Bureau, under grant CWB WBG-6.

EVALUATION OF ERRORS IN THE GRAPHICAL RECTIFICATION OF SATELLITE PHOTOGRAPHS

Tetsuya Fujita

Department of the Geophysical Sciences

The University of Chicago

Chicago, Illinois

Abstract. In order to investigate the proper design of the grid systems used in gridding or rectifying satellite pictures, an evaluation of errors from various sources has been made. It was found that the discrete grid intervals of both height and tilt are of vital importance in determining final accuracy. The rotation of the grid around the exposure subpoint is found to be permissible unless an accuracy of 0.1^{o} is required. Where accuracy requirements permit, the author's OEC height grids may be replaced by ZE height grids which are less complicated and much easier to use. This change also permits the use of perspective height and tilt grids with less than 0.2^{o} error. An evaluation of the gridding error due to the uncertainty of the spin-axis points revealed that it may be almost entirely eliminated by adopting a coupled rotation of the principal lines.

1. INTRODUCTION

The TIROS meteorological satellites launched during the past have transmitted back a large number of cloud pictures. These pictures were received solely at the ADC stations until recently when an initial test of the Automatic Picture Transmission (APT) was made on board the TIROS VIII space craft. In view of the progress in the improvement of the APT images, which can be obtained directly at any station within the readout range of the satellite, we expect that a large number of people will have

access to the satellite pictures received at real time bases.

Both these pictures and those received later from the ADC stations, are analyzed with varying degrees of accuracy required by the individual user. Three basic considerations in gridding a series of the pictures are (a) the accuracy requirements of the user, (b) the time required to analyze the pictures, and (c) the proper equipment and expenses for the analysis. These three are closely interrelated and cannot be discussed independently.

Geographic grids composed of longitude and latitude lines can be constructed by either computer or graphical methods. Examples of the former are the G 15 computer grids produced at the ADC stations operationally by the ARACON Geophysics Company and the 7090 computer grids produced for research purposes by the Meteorological Satellite Laboratory, U.S. Weather Bureau.

Graphical methods require more analysis time than computer methods; nevertheless, they have two basic advantages. First of all, they only require a library of grids and charts which are ready to be distributed. Secondly, the accuracy achieved by graphical methods is much greater than that by computer methods. Furthermore, the basic work performed by graphical methods increases the accuracy of input quantities for computers.

This paper discusses the applications of graphical methods to the gridding of satellite pictures of a required accuracy. If, for instance, an accuracy of 0.1^{o} in geocentric angle (6 n mi) is required within the area of a 15^{o} subsatellite distance, the so-called Precise Fujita Method (1963a) should be applied. A considerable amount of time is necessary before reaching rewarding results. It would take a whole day to complete geographic grid lines at one-degree intervals on a few images. The Approximate Fujita Method, however, permits one to complete a five-degree geographic grid in about 30 minutes with an expected accuracy of 0.5^{o} in geocentric angle. This is the average accuracy being obtained by the 7090 computer method. It should be noted, therefore, that the analysis time increases in inverse proportion to the square of the expected error below 0.5^{o}. The natural limit of accuracy is about 0.1^{o} since the electronic distortions vary from frame to frame making it very difficult to correct them entirely.

2. BASIC GRID SYSTEMS FOR GRAPHICAL METHODS

In principle, geographic gridding of cloud photographs is simply the usual transcription of latitude and longitude intersections from a chart to a picture using two corresponding grid overlays. One overlay grid is a projection of the other so that one matches the scale and projection of the picture while the other matches the chart (Fig. 1).

Theoretically, there are two basic systems of grids which may be called the combined grid system and the independent grid system. The former is characterized by a unique grid defined either on an image or on the earth, and the corresponding grids vary according to the combination of both the image tilt and the satellite height. To meet the operational requirements of quick gridding, Glaser (1960) developed and Hubert (1961) discussed a combined grid system which includes a unique grid defined on the earth and corresponding grids on the image.

So far, the other type of the combined grid system, using a unique grid placed on an image, has not been worked out. In this case the grids on the earth should change as a function of the tilt and the height combined. An advantage of the combined grid system is an easy gridding which can be performed by using a small number of grids if the satellite height does not vary appreciably. For height and tilt ranges which require a combination of m heights and n tilts, the total number of grids in the combined grid system is expressed by $m \times n$.

For a precise graphical method, which naturally requires very small height and tilt increments, the total number of grids needed in the combined grid system is too large to be practical. Both Fujita's Precise and Approximate Methods (1961) (1963a) (1963b) utilize an independent grid system characterized by two sets of grids, one is defined on the earth as a function of height and the other, on the image as a function of tilt. The total number of grids required in analyzing the combination of n heights and m tilts is only $m+n$, which is considerably less than $m \times n$, the total number needed in the combined grid system.

In fact, Fujita's Grids include 50 height grids covering the height range of 500-990 km and 100 tilt grids covering the 0-99^{o} tilt, thus resulting in a total of 150 grids. If the same combination of heights and tilts were obtained by using the combined grid system, it would require a library of 5,000 grids. This number prohibits the application of the

combined grid system in a precise graphical method. Even if the independent grid system is used, the total number of grids is fairly large. It is, therefore, necessary to investigate the discrete intervals of the grids required to obtain the desired accuracy of picture-gridding.

3. INFLUENCE OF SATELLITE HEIGHT

The heights of the meteorological satellites tabulated by NASA in a Definitive AT Map are known to within one kilometer. If the exposure time of a picture is determined within about one sec., for instance, the accuracy of the exposure subpoint should be about seven kilometers.

The subsatellite distance (d), the geocentric angle of a point measured from the subsatellite point, determined from a photograph as a function of the altitude (H), nadir angle of view (η), and the local radius of curvature (ρ) are expressed implicitly as

$$\sin(\eta + d) = \frac{\rho + H}{\rho} \sin\eta \quad . \tag{1}$$

Differentiating the subsatellite distance with respect to H, while keeping η and ρ constant, we have

$$\left(\frac{\partial d}{\partial H}\right)_{\eta,\rho} = \frac{\sin\eta}{(\rho + H)\sqrt{\cos^2\delta_H - \sin^2\eta}} \quad , \tag{2}$$

where δ_H denotes the dip, the depression angle of the apparent horizon. For the satellite height of 700 km, the average TIROS height, the error in the subsatellite distance is calculated as shown in Table I.

Table I. The error of the subsatellite distance (in degrees of geocentric angle) per 10 km of height error. (Satellite height 700 km)

η	0	30	50	55	58	60
d	0.0	3.7	8.2	10.4	12.2	14.0
$10\left(\frac{\partial d}{\partial H}\right)_{\rho,\eta}$	0.00	0.05	0.13	0.18	0.23	0.28

The tops of high clouds beyond 10 km msl may be found practically everywhere over the earth, making it almost impossible to place a height grid on each cloud top of varying height. The natural limitation of accuracy at the 10^{o} subsatellite distance is considered as about 0.2^{o} due to the variability of the cloud tops.

The local curvature of the earth also contributes to the error in the subsatellite distance. The error is obtained by differentiating Eq. (1) with ρ, thus

$$\left(\frac{\partial d}{\partial \rho}\right)_{H,\eta} = \frac{-H}{\rho(\rho+H)} \tan(\eta + d) . \qquad (3)$$

The error in the subsatellite distance is, therefore, written as

$$\Delta d = \frac{-H\,\Delta\rho}{\rho(\rho+H)} \tan(\eta + d) ,$$

where $\Delta\rho$ is the deviation of the local radius of curvature from the mean radius of the earth. The extreme values of the deviations, +32.2 km and -32.2 km, exist along the meridians at the poles and on the equator, respectively. Table II reveals, however, that the error due to the radius of curvature is approximately the same as that created by a 3-km error in height.

Table II. The error of the subsatellite distance (in degrees of geocentric angle) due to 32.2 km deviation of the local radius of curvature. Satellite height is assumed to be 700 km.

η	0	30	50	55	58	60
	0.00	0.02	0.05	0.06	0.09	0.10

The heights of clouds above the standard surface of the earth, which vary between 0 and 15 km, would therefore introduce a much larger error than would the curvature of the earth. The natural limit of the discrete intervals of the height grids should be considered as about 10 km, while the spherical approximation of the earth is valid as long as the position of the satellite is expressed in terms of the geodetic latitude, the longitude, and the height above the standard surface of the earth.

4. ROTATION OF THE PRINCIPAL LINE

For the purpose of analysing successive satellite pictures taken along its subpoint track the oblique equidistant projection chart introduced by Fujita (1963) is commonly used. In the OEC Projection, the distances along the projection equator and the projection meridian as defined in the original article are preserved upon projection. The horizontal angles and the subsatellite distances are distorted in all other directions. When a grid is placed on the OEC chart, it must be rotated to a certain extent until the principal line on the grid coincides with that drawn on the OEC chart.

To evaluate the error resulting from this rotation a Zenithal Equidistant (ZE) and OEC charts were superimposed on a common origin shown in Fig. 2. Suffixes z and o denote the points and lines on these charts, respectively. The errors in radial (E_ϵ) and tangential (E_γ) directions can be written as

$$E_\gamma = (y_z - y_o)\cos\psi + (x_o - x_z)\sin\psi \qquad (4)$$

$$E_\epsilon = (y_z - y_o)\sin\psi + (x_o - x_z)\cos\psi \ , \qquad (5)$$

where ψ is the horizontal angle measured from the projection equator. Solving a plane triangle and a spherical triangle we obtain

$$y_z = d \sin\psi \quad , \quad x_z = d \cos\psi$$

and

$$\sin y_o = \sin d \sin\psi \quad , \quad \tan x_o = \tan d \cos\psi \quad ,$$

which are then put into Eqs. (4) and (5). Since the maximum value of d is the dip, δ_H, viewed from the satellite height, it is safely assumed to be less than 30^o for the present TIROS heights, permitting us to neglect d^5 or higher order terms. Thus we finally obtain

$$E_\gamma \cong \frac{d^3}{24} \sin 2\psi \,(3-\cos 2\psi) \quad , \tag{6}$$

and

$$E_\epsilon \cong \frac{d^3}{24} \sin^2 2\psi \quad . \tag{7}$$

These are the errors expected when a grid constructed on a ZE projection is placed on an OEC chart and rotated by ψ until the principal lines on the grid and the chart coincide. The maximum tangential error takes place at $\psi = 54^o$, and the radial error, at 45^o (see Fig. 3).

To avoid this tangential error, Fujita's Precise Method employs a set of OEC height grids which need to be rotated only a maximum of 5^o in order to match the principal lines. The errors in such a small angle of rotation are expressed by

$$\Delta E_\gamma = \left(\frac{\partial E_\gamma}{\partial \psi}\right)_d \Delta\psi = \frac{d^3}{12} \Delta\psi \,(-2\cos^2 2\psi + 3\cos 2\psi + 1) \tag{8}$$

$$\cong \frac{d^3}{138}(-2\cos^2 2\psi + 3\cos 2\psi + 1), \quad \text{for } \Delta\psi = 5 \text{ deg} \tag{9}$$

and

$$\Delta E_\epsilon = \left(\frac{\partial E_\epsilon}{\partial \psi}\right) \Delta\psi = \frac{d^3}{12} \Delta\psi \sin\Delta\psi \tag{10}$$

$$\cong \frac{d^3}{138} \sin 4\psi \quad . \qquad \text{for } \Delta\psi = 5 \text{ deg} \qquad (11)$$

As tabulated in Table III, the errors are insignificant when the subsatellite distance is small since they are proportional to the third power of d .

Table III. Maximum error (in degrees of geocentric angle) tabulated as a function of the subsatellite distance.

Subsatellite distance	0	10	20	30	40
Satellite height (in km) required to photograph above distance	0	100	400	1,000	2,000
Tangential error of ZE grid	0.00	0.04	0.33	1.11	2.62
Tangential error of OEC grid	0.00	0.00	0.06	0.27	0.55
Radial error of ZE grid	0.00	0.01	0.10	0.35	0.83
Tangential Error of OEC grid	0.00	0.00	0.02	0.06	0.14

This table shows that the OEC height grid used in Fujita's Precise Method can be switched to the ZE height grid if one is satisfied with an accuracy of 0.3° rather than 0.1° as originally intended for the precise analysis. Further, a ZE grid system may be constructed in the form of the perspective height and the perspective tilt grids as introduced by Fujita (1963) because they can be rotated freely.

As an inevitable consequence of plotting the subsatellite points on the rotating earth coordinates, the TSP track appears to deviate from the projection equator due to the two forces introduced by the change in coordinates. They are

$$F_1 = -2V^{TSP}w \sin\phi \quad \text{(coriolis force)} \qquad (12)$$

and $$F_2 = -\frac{1}{2} R w^2 \sin 2\phi \ . \qquad \text{(centrifugal force)} \qquad (13)$$

where R denotes the radius of the earth. The former apparently bends the TSP track toward the right in the Northern Hemisphere; and the latter, acting along the meridian toward the equator, not only bends the TSP track toward the equator but also reduces the speed of the subsatellite point to its minimum value at the northern- and southern-most latitudes. The short segments of the TSP track thus deviate from the project equator by the amount in geocentric angles,

$$\Delta y \cong \sin i \ \frac{w_e}{w_s} \ u' \cos (u_e + u') \ , \qquad (14)$$

where, i denotes the inclination of orbit; w_e, the angular velocity of the earth's rotation; w_s, that of the satellite in orbit; u_e, the argument of satellite at the projection-equator crossing; and u' the argument of satellite past the projection-equator crossing. As a result of this effect we have to expect that a TSP is up to about 2^o off from the projection equator causing an error which does not normally exceed 0.2^o.

5. INFLUENCE OF TILT

Although satellite photographs cover a continuous range of tilts between zero and about 100^o, it is not practical to construct a set of tilt grids at very close intervals. It is necessary, therefore, to investigate these discrete intervals as a function of the required accuracy of picture-gridding. First we differentiate Eq. (1) with respect to η while keeping H and ρ constant. Thus we obtain

$$\left(\frac{\partial d}{\partial \eta}\right)_{H,d} = \frac{\cos \eta}{\sqrt{\cos^2 \delta_H - \sin^2 \eta}} - 1 \ , \qquad (15)$$

where δ_H is the dip viewed from the satellite.

Table IV. Error (in degrees of geocentric angle) of the subsatellite distance due to one-degree error in the nadir angle.

nadir angle	0	30	50	55	58	60
$\left(\frac{\partial d}{\partial \eta}\right)_{H,\rho} \times 1.0°$	0.11	0.15	0.35	0.53	0.75	1.00

It should be noted that the error in subsatellite distance due to the nadir angle error exists even at the subpoint. In both combined and independent grid systems, extra care is exercised to bring the principal point on the image (IPP) and on the earth (TPP) together; however, the discrete intervals of tilt may cause serious error near the subpoint where the analyst expects to obtain the best accuracy.

Now we superimpose the grid with true tilt τ and the other with $\tau + \Delta\tau$, the tilt of the available grid (Fig. 4). Since the grids are used in such a manner that the principal point (IPP) on the true image coincides with the point on the principal line where the nadir angle is identical to the tilt, then the distance on the image between IPP and IPP' is equal to $f\,\Delta\tau$. The nadir angle error ($\Delta\eta$) thus created is obtained by solving the equation

$$\tan\left\{(\eta-\tau)-\Delta\tau\right\} + \tan\Delta\tau = \tan\left\{(\eta-\tau)-\Delta\eta\right\} ,$$

which is solved by first expanding into power series and then neglecting second and higher orders in $\Delta\tau$. Thus we have

$$\left|\Delta\eta\right| = \sin^2\epsilon\ \Delta\tau , \qquad (16)$$

where ϵ denotes the radial angle on the image measured from the principal point. This equation reveals that the error in the nadir angles measured on the principal plane is proportional to the square of the sine of the radial angle measured from the image principal point.

Next we combine Eq. (16) with Eq. (15) after changing the latter into a finite difference form, thus

$$\Delta d = \Delta\tau \left(\frac{\cos\eta}{\sqrt{\cos^2\delta_H - \sin^2\eta}} - 1 \right) \sin^2(\eta - \tau) \quad , \qquad (17)$$

where $\eta-\tau$ is identical to ϵ, since we are dealing with the nadir angles measured on the principal plane. This equation permits us to compute the maximum error in the subsatellite distance due to the use of a grid with the tilt deviating by $\Delta\tau$ from the true tilt. When the proper tilt grid is selected, $\Delta\tau$ should not exceed one half of the discrete tilt intervals. With the use of Table V, the errors resulting from these intervals can be obtained by simply multiplying the values in the table by the one-half of the intervals.

Table V. Error (in degrees of geocentric angles) of the subsatellite distance (viewed from the 700-km height) due to 1^o difference between the true tilt and the grid tilt. The table shows the maximum errors which take place on the principal line. The values which appear outside the 100^o field of view are indicated with * symbols.

Nadir angle	0	30	50	55	58	60
Tilt 0	0.00	0.04	0.21	0.35*	0.54*	0.75*
Tilt 20	0.01	0.00	0.09	0.18	0.28	0.41
Tilt 40	0.05	0.00	0.01	0.04	0.08	0.12
Tilt 60	0.08*	0.04	0.01	0.01	0.00	0.00
Tilt 80	0.11*	0.09	0.09	0.10	0.10	0.12
Tilt 90	0.11*	0.11*	0.15	0.18	0.21	0.28

6. SUMMARY OF GRAPHICAL GRIDDING CAPABILITIES

It has been explained that graphical methods can be used in gridding satellite pictures with various degrees of accuracy, which is required by each user under various circumstances.

The estimate of the error heretofore attempted now permits us to tabulate the grid systems and the number of charts required in gridding photographs with given accuracies. Because of the variability of cloud heights, it is not practical to utilize the height intervals of less than 10 km, which limits the gridding accuracy to 0.1^{o} or worse. In considering the fact that the determination of both time and image principal line might double the error, it is not realistic to assume that an accuracy better than 0.1^{o} geocentric angle is obtained through any graphical method.

As shown in Table VI, the intervals of both height and tilt grids as well as the limits of grid rotation are determined by the accuracy required; thus the total number of grids required to obtain such accuracies is estimated. It is evident that the number of the combined grids increases very rapidly as the error decreases, making it almost impossible to construct the grids when an accuracy higher than 0.3^{o} is required. On the other hand, the independent grids can be constructed to achieve about 0.1^{o} accuracy without increasing the number of charts beyond about 150.

Table VI. Showing the height and tilt intervals required to accomplish a gridding of satellite pictures with given accuracies. The range of satellite height, 500-1000 km; and that of tilt, $0\text{-}100^{o}$ are used in estimating the total number of charts.

Accuracy required (degrees)	Height intervals (km)	Tilt intervals (degrees)	Limit of rotation (degrees)	Total number of charts needed for Independent grids	Combined grids
1.0	80	7.5	90	7+ 14= 21	98
0.5	40	4	90	13+ 26= 39	338
0.3	25	2	90	21+ 51= 72	867
0.2	10	1	90	51+ 101= 152	5,151
0.1	10	1	5	51+ 101= 152	51,510

There are four grid systems available for researchers who wish to rectify or grid a series of satellite photographs. As shown in Table VII each of the grid systems may

result in the specified maximum error due to the causes discussed in sections 3, 4, and 5. Additional errors should always be expected because of the errors in time determination and in orienting the principal line on each image. This subject will be discussed in the following section.

Table VII. The list of the rectification grids available from various sources. The first and the fourth belong to the combined grid system, and the second and the third to the independent grid system. Possible error applies to the 700-km height and 58° nadir angle. * indicate error for satellite height 450 miles.

Grid systems	Grids on the MAP	Grids on the IMAGE	Limit of ROTATION	Possible ERROR in geocentric angle
Canadian grids Glaser (1960)	Transfer grid one grid on Oblique Mercator Chart	Perspective grids 450-mi height 2.5-deg tilt intervals	90°	*0.4
Precise grids Fujita (1961)	OEC Height grids 10-km intervals on OEC Chart	Tilt grids 1-deg intervals on distortion-free image	5°	0.1
APT grids Schwalb (1963)	Transfer grid one grid on OEC Chart	Perspective grids 25-mi height intervals 5-deg tilt intervals	90°	0.7
Approximate grids Fujita (1964)	ZE Height grids 10-km intervals on OEC Chart	Tilt grids Same as of the precise grids	90°	0.2

7. ERROR IN TIME AND PRINCIPAL LINE DETERMINATIONS

We have so far discussed the error in gridding due to discrete intervals of heights and tilts as well as to the inevitable rotation of the principal line on the grid. Additional errors in the determination of the following items result in added inaccuracy. They are: the exposure subpoint (or time), the tilt, the terrestrial principal line, and the image principal line. For details consult the articles by the author.

The exposure times of the direct readout pictures are known accurately so that the exposure subpoints are estimated with an accuracy better than 0.1° geocentric angle. For tape-mode pictures, the accuracy in time determined from the 550-cycle satellite clock signals is generally very high, permitting the determination of exposure subpoint with reasonable accuracy. In case no satellite clock signal is available, it is usual to determine the exposure time using the tilt computed from pictures with well-defined horizons.

For convenience we define the axial point as the subsatellite point where the minimum nadir angle takes place in each orbit. The argument of satellite measured from the axial point in the direction of orbital motion is then termed the axial anomaly, v_a . For a circular orbit we may write $v_a = w_s (t - t_o)$, where w_s denotes the angular velocity of the satellite orbital motion. Using the conventional symbols, η_o for the minimum nadir angle, and t_o , for the time of the minimum nadir angle we assume that τ is equal to η_s , the satellite nadir angle in order to write

$$\cos\tau = \cos\eta_o \cos w_s (t - t_o)$$

or

$$t = t_o + \frac{1}{w_s} \cos^{-1} \frac{\cos\tau}{\cos\eta_o} \quad , \tag{18}$$

and obtain the error as

$$dt = \left(\frac{\partial t}{\partial t_o}\right) dt_o + \left(\frac{\partial t}{\partial \eta_o}\right) d\eta_o$$

$$= dt_o - \tan\eta_o \left(\frac{\cos^2\eta_o}{\cos^2\tau} - 1\right)^{-\frac{1}{2}} \frac{d\eta_o}{w_s} \quad . \tag{19}$$

It is evident that the error in the time of minimum nadir angle is directly related to the exposure time. The contribution of the minimum nadir angle error to the time error, which is given by the second term in Eq. (19), approaches infinity when either $\eta_o = 90^{\circ}$ or $\eta_o = \tau$. It is, therefore, not recommended to determine the

exposure time from the picture tilt under these circumstances. The best time accuracy is obtained on the other hand if we select the frame with $\tau = 90^{\circ}$. In such a case Eq. (19) is reduced simply to

$$dt = dt_o \quad , \tag{20}$$

thus the error in the minimum nadir angle does not contribute to the time error. In TIROS cases, η_o is normally kept under 30°. The method of spin-axis determination devised by Fujita (1961) produces almost 0.3° scatter in geocentric angle or 0.3° minimum nadir angle uncertainty ($d\eta_o$). One might then expect an equivalent time error of as much as 5 seconds from the first term of Eq. (19) only. It should be noted that a landmark is needed to increase time accuracy beyond this limit.

The orientation of the terrestrial principal line is also influenced by the accuracy of the position of the spin-axis point. We shall now estimate the orientation error as a function of errors in η_o and t_o. Solving the spherical triangle formed by the spin-axis point, the subsatellite point, and the minimum nadir angle subpoint, we write

$$\sin\alpha = \csc\tau \sin\eta_o \tag{21}$$

and

$$\cos\alpha = \cot\tau \tan v_a \quad , \tag{22}$$

where $v_a = w_s(t-t_o)$ and α denotes the azimuth of the principal line measured from the subpoint heading on the fixed earth. The total error due to the uncertainty in both η_o and t_o is now expressed as

$$d\alpha = \left(\frac{\partial\alpha}{\partial\eta_o}\right)d\eta_o + \left(\frac{\partial\alpha}{\partial t_o}\right)dt_o \quad ,$$

which can be obtained by differentiating Eqs. (21) and (22), thus

$$d\alpha = \frac{\cos \eta_o}{\sqrt{\sin^2 \tau - \sin^2 \eta_o}} d\eta_o + \frac{\sec^2 v_a}{\sqrt{\tan^2 \tau - \tan^2 v_a}} w_s \, dt_o \, . \qquad (23)$$

The range of variation of v_a extends between 0^o and 360^o, while that of τ, between η_o and 180^o. The worst errors in α should, therefore, take place near the axial point of each orbit where $\tau \cong \eta_o$, and also when η_o is very small. These combinations result in an extreme uncertainty of the principal line orientation in the vicinity of the axial point, especially when η_o is small. Under certain circumstances, such an error may exceed 10^o or even 30^o.

When the subsatellite point is very far from the axial point, the error given in Eq. (23) is small. At the same time a well-defined apparent horizon should appear on the image to be gridded. In such a case the orientation error in the principal line on the image and on the OEC chart can be brought to under one degree of azimuth.

If the subsatellite point is near the axial point, on the other hand, the exact orientation of the principal line cannot be obtained, due to the fact that so far there exists no method to determine the spin-axis point with an accuracy of 0.1^o; moreover, the spin-axis point in the celestial coordinates may move a few tenths of a degree during one orbit.

As a result of this inevitable error, it is not feasible to determine the principal lines on the images and on the OEC chart independently. That is to say, the principal line on either the image or the OEC chart should be obtained first, then transferred to the other. By doing this, the same orientation error is likely to be included in such a way that the positions of the objects on both the image and the chart maintain the same relative positions while both principal lines rotate in the same direction and with the same angle due to the error in the spin-axis point. Equation (23) acts in favor of this process, since a large error is expected only when the tilt is small. If the tilt is only a few degrees, for instance, large rotation angles of the image and chart primary lines may be permissible as long as they are the same in direction and amount. Such rotation of the principal lines is called coupled rotation.

Coupled rotation is very important in gridding photographs without horizon. In performing this, we have to first determine the spin-axis points using the most accurate data sources including:

(A) Fujita's (1963a) method of spin-axis determination using the frames belonging to the picture series to be analyzed;

(B) spin-axis declination and right ascension as tabulated in Goldshlak (1962-) or NASA's (1960-) Definitive AT Map.

The former gives the spin-axis points on the OEC and the latter can be converted immediately into terrestrial coordinates. Once the spin-axis points are determined, they should be used throughout the analysis to allow coupled rotation. There are two basic methods in which coupled rotation is implicitly utilized: The principal points are used in one method and the sun angles in the other.

The principal point method, originally introduced by Fujita (1961), may be performed by approximating the principal lines with straight lines connecting the spin-axis points and the corresponding subpoints. For the difference between the principal and primary lines, as well as for an account of the method in detail, one should refer to the author's articles. Figure 5 represents the straight principal lines which may be approximated for the low-tilt pictures that do not include the apparent horizon. The terrestrial principal points (TPP) are then located on each principal line, using the nadir angle chart. Since the Definitive AT Map produced by NASA includes the longitudes and the latitudes of picture centers (TPP) at one-minute intervals, one may as well plot these points on the OEC. As shown in Fig. 5, the TPPs plotted from the Definitive AT Map and those obtained from the straight-line approximation nearly coincide.

When the interpolation of the exposure subpoints (TSPs) and the TPPs is completed by using the predetermined exposure time, the TPPs on the OEC may be regarded as the landmarks or the survey points, which include the uncertainty resulting from the time error expressed in Eq. (20). By placing a proper height grid on the exposure subpoint, the TPPs are quickly transferred onto a proper tilt grid so that the distortion-free fiducial grid can be rotated around its IPP (correctly IPM) until the IPPs on the tilt grid and the distortion-free fiducial grid coincide. Through these processes, we are able to perform coupled rotations with an accuracy here of 1^{o} or better while examining the relative positions of IPPs obtained from the photographs and from the OEC chart.

Ideally, they should coincide, but we often find some irregular variations due to the inaccurate spin-axis points and the nutation of the vehicle's spin-axis.

The Sun-angle Method, which has not been used successfully due to the erratic appearance of the sun angles on the monitor display, can also be used in determining the image principal line based upon the principle of the coupled rotation. The sun angle indicated on the monitor display for each frame is the tangential angle γ^{SN} between the primary sun line and the sun-line reference which forms an angle, C, with the test-target reference line as shown in Fig. 6. The tangential angle on the test target is included in all distortion-free fiducial grids so that the orientation of the principal line can be expressed by the angle γ^{PP} . Under the heading of picture sun-angle, the Definitive AT Map tabulates at one-minute intervals the spin angle μ of the principal line measured from the anti-solar direction. We may thus write the tangential angle of the principal line,

$$\gamma^{PP} = C + \gamma^{SN} + 180 - \mu$$

$$= \gamma^{SN} - \mu + 180 + C \qquad (24)$$

Coupled rotation can be performed only if γ^{PP} and μ are obtained from the same spin-axis data, that is, the angle γ^{PP} or the orientation of the image principal line should not be obtained from the image but should be computed from the spin-axis and the subpoint data which are used in computing μ . In other words, the principal line oriented in the direction of γ^{PP} computed from Eq. (24) matches the terrestrial principal line drawn on the OEC chart. The error in γ^{PP} is caused only by the inaccuracy in the sun angle γ^{SN}.

The two methods of determining the principal lines on the image and the chart will permit us to determine the lines with an accuracy no less than that which could be obtained by using the well-defined horizon. Therefore, the gridding accuracy of the pictures with and without apparent horizons may be considered practically the same, and the higher the accuracy of the spin-axis point the better the result. It should be kept in

mind that the exposure subpoint determined from the known spin-axis point may include up to about 0.5^{o} error unless one or more landmarks are used. With their use, the error in the exposure subpoint is usually reduced to 0.1^{o} geocentric angle.

8. CONCLUSION

It has been shown here that errors in gridding or rectifying satellite pictures are caused mainly by the size of the discrete grid intervals, rotation of principal line on the OEC chart, error in the spin-axis point, and uncoupled rotation of the principal lines.

Despite the fact that the author's Precise Rectification Method is designed to minimize these errors plus those caused by lens and electronic distortions, it is feasible to simplify the grids and the working procedures if less accuracy is still satisfactory. If we somehow eliminate the electronic and lens distortions, the rotation of the principal line may be performed up to 90^{o} without introducing more than 0.2^{o} error. The error estimate thus justifies the use of any grid on a ZE projection which can be rotated until the principal lines on the grid and on the chart coincide.

The error resulting from the discrete intervals of both height and tilt was thoroughly investigated, leading to an estimation of the number of grids required in gridding pictures with given accuracies. The independent grid system was found to be superior to the combined grid system for accurate rectification involving pictures taken from various altitudes and large tilt ranges.

The equations of error resulting from the uncertainty in the position of the spin-axis point have been solved. They indicate that this inevitable error appreciably influences the determination of the exposure time and the orientation of the principal line, especially when the subsatellite point is located near the axial point.

Although graphical methods of analyzing satellite pictures are time consuming, the time is a function of accuracy requirements. The gridding time may be cut down to less than 30 minutes per frame with the least stringent accuracy requirements.

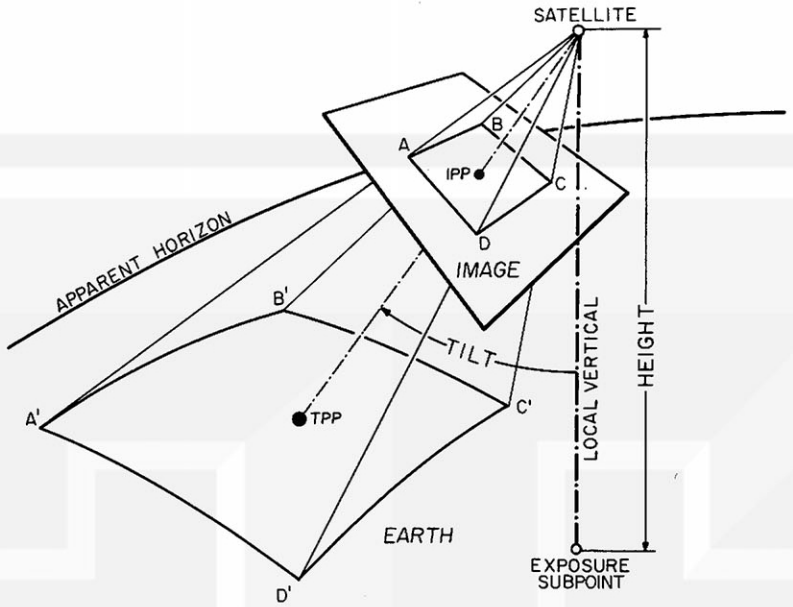

Fig. 1. Schematic diagram showing a grid on the image and a corresponding grid on the earth. In the combined grid system, a unique grid on the earth is projected onto the image as a function of the height and tilt combined. A significant reduction in the number of grids is made by adapting the independent grid system in which the grids on both the image and the earth are changed as a function of tilt and the height, respectively.

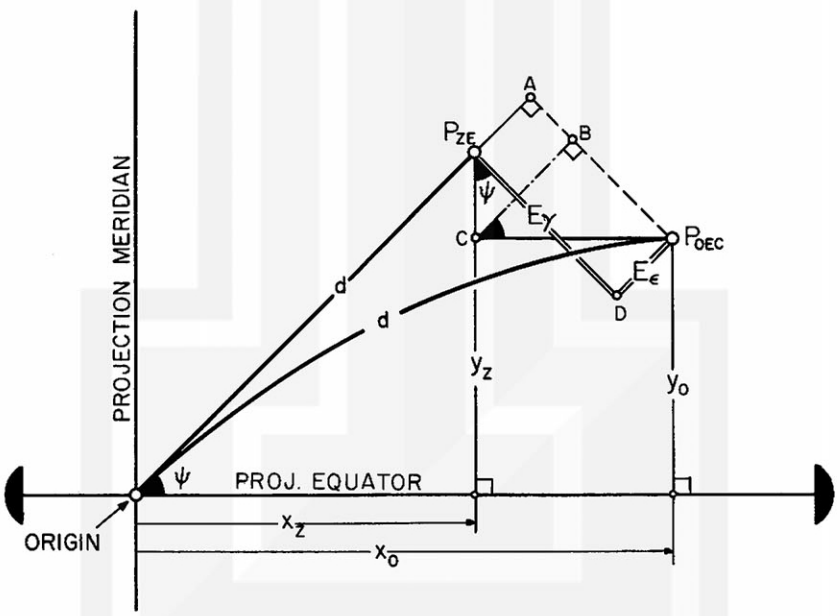

Fig. 2. The tangential and the radial errors caused by using a grid in ZE projection superimposed upon an OEC projection chart. For a subsatellite distance d and a horizontal angle ψ, the ZE and OEC give two points, P_{ZE} and P_{OEC}, thus creating an error which is proportional to the third power of d.

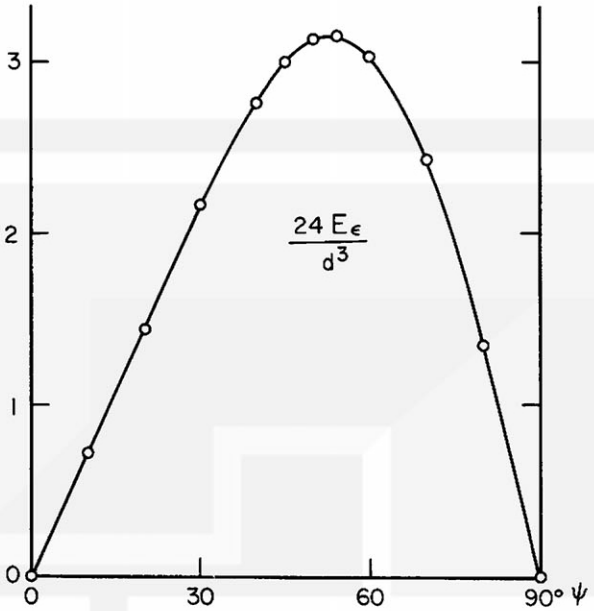

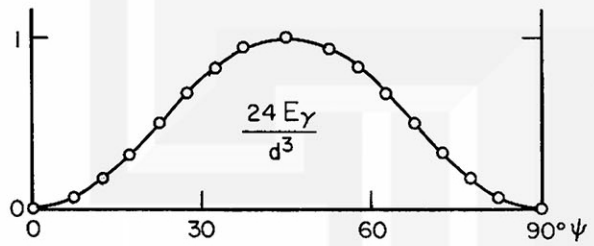

Fig. 3. The tangential and radial error plotted as a function of the horizontal angle measured from the projection equator. The maximum error in the tangential direction takes place when $\psi = 54^\circ$, and that in the radial direction, when $\psi = 45^\circ$. The maximum tangential error is 3.12 times the maximum radial error.

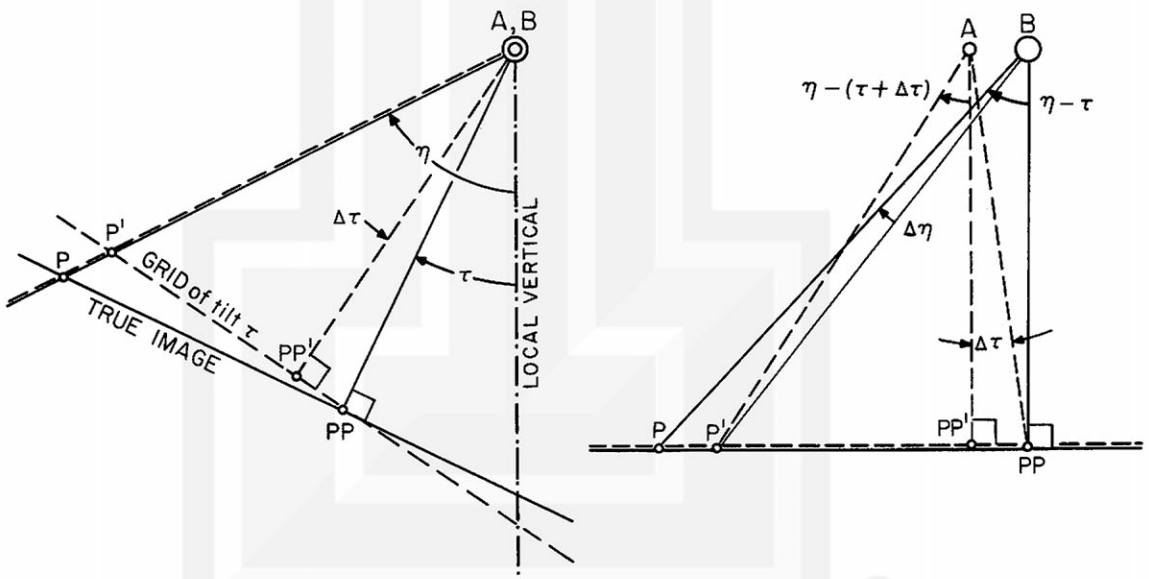

Fig. 4. Computation of error caused by the use of a tilt grid, the tilt of which is larger by $\Delta\tau$ than that of the true image tilt. The principal point (PP) of the true image is adjusted so that it coincides with the point on the grid principal line whose nadir angle represents the true image tilt. The left figure shows the grid and image relationship in the true object space, and the right, the nadir angles P and P' on the grid, which should be identical in the true object space.

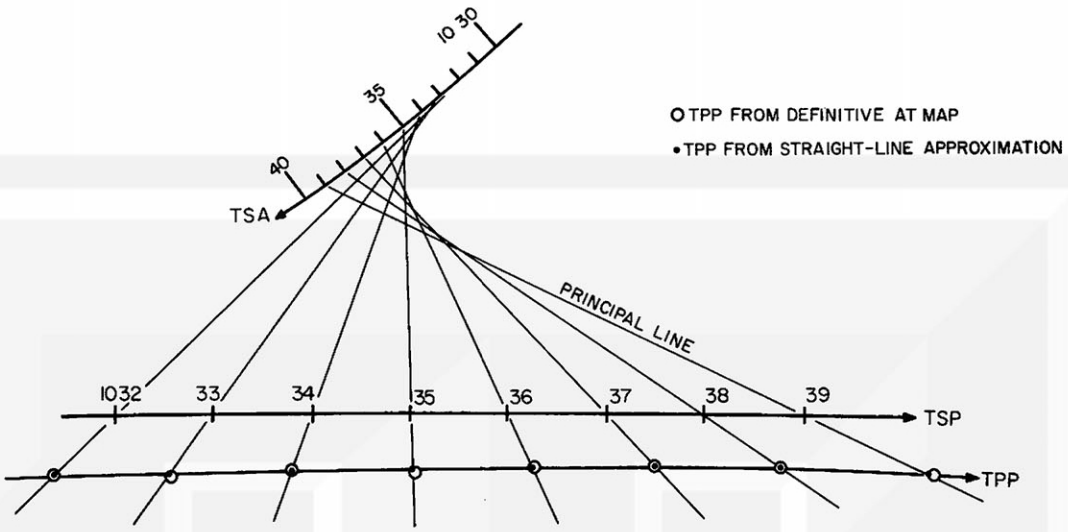

Fig. 5. Determination of the principal line and the principal points on an OEC chart under the straight line approximation which is applicable when the satellite nadir angle is less than 15^{o}. Abbreviations: TSA - terrestrial spin-axis point, TSP - terrestrial subpoint, and TPP - terrestrial principal point. The TSAs are obtained from the right ascension and declination of the celestrial spin-axis point. The TPPs can be obtained on each principal line using straight-line approximation or plotted from the Definitive AT Map.

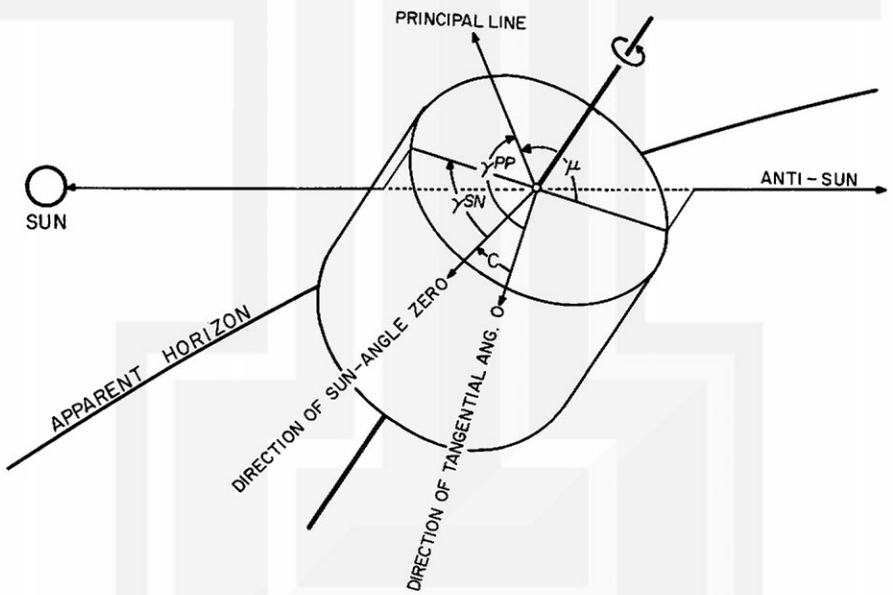

Fig. 6. Geometry in computing the tangential angle of the image principal line by using the sun angle. Symbols: μ -spin angle of the principal line measured from the anti-sun line, γ^{PP}-tangential angle of the principal point, γ^{SN} -tangential angle of the sun-line measured from the direction of sun-angle zero, also called sun angle, and C - the tangential angle of the direction of sun-angle zero. If the sun angle is known as a function of the frame, the principal line on each frame can be computed without using the apparent horizon.

REFERENCES

Fujita, T., 1961: Outline of a technique for precise rectification of satellite cloud photographs, Mesometeorology Research Paper No. 3, Chicago Univ.

Fujita, T., 1963a: A technique for precise analysis of satellite data; volume I-photogrammetry, Meteorolotical Satellite Laboratory Report No. 14, U.S. Weather Bureau.

Fujita, T., 1963b: A technique for precise analysis of satellite photographs, Mesometeorology Research Paper No. 17, Chicago Univ.

Glaser, A.H., 1960: A system for the meteorological use of satellite television observations, IV, GRD Research Notes No. 36, Geophysics Research Directorate.

Goldshlak, L., 1962-63: TIROS III, IV and V attitude summaries, ARACON Geophysics Co., Concord, Mass.

Hubert, L. F., 1961: Canadian grids for TIROS I; additional orientation data; errata, Supplement to Meteorological Satellite Laboratory Report No. 5, U.S. Weather Bureau.

NASA, 1960: TIROS definitive AT maps.

MESOMETEOROLOGY PROJECT ----- RESEARCH PAPERS

(Continued from front cover)

16. Preliminary Result of Analysis of the Cumulonimbus Cloud of April 21, 1961 - Tetsuya Fujita and James Arnold

17. A Technique for Precise Analysis of Satellite Photographs - Tetsuya Fujita

18. Evaluation of Limb Darkening From TIROS III Radiation Data - S.H.H. Larsen, Tetsuya Fujita, and W. L. Fletcher

19. Synoptic Interpretation of TIROS III Measurements of Infrared Radiation - Finn Pedersen and Tetsuya Fujita

20. TIROS III Measurements of Terrestrial Radiation and Reflected and Scattered Solar Radiation - S.H.H. Larsen, T. Fujita, and W.L. Fletcher

21. On the Low-level Structure of a Squall Line - Henry A. Brown

22. Thunderstorms and the Low-level Jet - William D. Bonner

23. The Mesoanalysis of an Organized Convective System - Henry A. Brown

24. Preliminary Radar and Photogrammetric Study of the Illinois Tornadoes of April 17 and 22, 1963 - Joseph L. Goldman and Tetsuya Fujita

25. Use of TIROS Pictures for Studies of the Internal Structure of Tropical Storms - Tetsuya Fujita with Rectified Pictures from TIROS I Orbit 125, R/O 128 - Toshimitsu Ushijima

26. An Experiment in the Determination of Geostrophic and Isallobaric Winds from NSSP Pressure Data - William Bonner

27. Proposed Mechanism of Hook Echo Formation - Tetsuya Fujita with A Preliminary Mesosynoptic Analysis of Tornado Cyclone Case of May 26, 1963 - Tetsuya Fujita and Robbi Stuhmer

28. The Decaying Stage of Hurricane Anna of July 1961 as Portrayed by TIROS Cloud Photographs and Infra-red Radiation from the Top of the Storm - Tetsuya Fujita and James E. Arnold

29. A Technique for Precise Analysis of Satellite Data;Volume II - Radiation Analysis, Section 6. Fixed-Position Scanning - Tetsuya Fujita